

Experimental and numerical investigation of highly absorbing nonlinear organic chromophores

E. Parilov^{*a} and M. J. Potasek^{a,b}

^aSimphotek, Inc., 211 Warren St., Newark, NJ 07103

^bCourant Institute of Mathematical Sciences, New York University, NY 10003

ABSTRACT

We have developed a mathematical/numerical framework based on computational transition modules and measured ultrafast laser light propagating through nonlinear materials. The numerical framework can be applied to a broad set of photo-activated materials and lasers, and can optimize photo-physical parameters in multi-photon absorbers. Two photon (TPA) processes are particularly useful in many applications including fluorescence imaging, optical data storage, micro-fabrication, and nanostructured quantum dots for optical limiters. Laser transmission measurements of the organic molecular chromophore, AF455-known TPA material-were taken with a 175 fs, $\lambda_0=780\text{nm}$, plane-polarized light pulses from Ti:S regenerative amplifier into a 5.1mm thick PMMA slab doped with the chromophore. The range of input energies (intensities) in this experiment was $0.01\mu\text{J}$ (0.97 GW/cm^2) to $25\mu\text{J}$ ($2.4 \times 10^3\text{ GW/cm}^2$). Experiments showed that for intensities beyond several μJ , the material did not saturate as predicted by traditional theory. We included excited-state absorption (ESA), as demonstrated by the absorption spectrum, which still could not account for the deviation. To understand this result we used our framework to show that an unexpected/unknown higher energy level was being populated. We calculated the entire experimental curve from $0.01\mu\text{J}$ (0.97 GW/cm^2) to $25\mu\text{J}$ ($2.4 \times 10^3\text{ GW/cm}^2$) and found excellent agreement with the experimental data.

Keywords: nonlinear optics, two-photon absorption, numerical calculation

1. INTRODUCTION

Photonics is becoming significant in many areas and may replace or augment electronics in many applications, such as silicon waveguide photonics [1], dye-sensitized photovoltaic cells for solar energy [2], nanostructured quantum dots for lighting [3], and rare-earth ions for displays [4]. Understanding and utilizing optical nonlinearities [5] is becoming a central topic in Photonics; for example, recent developments in technology have created faster and more intense lasers, from the visible to the far infrared [6], thus enabling multi-photon processes across a broad range of wavelengths from the visible ($\sim 0.4\text{-}0.6\mu\text{m}$) to the short ($0.8\text{-}2\mu\text{m}$), mid ($3\text{-}8\mu\text{m}$) and far ($>12\mu\text{m}$) infrared spectral regions. Two photon processes are particularly useful in many applications including fluorescence imaging [7], fluorescence microscopy in biology and medicine [8-9], optical data storage [10], micro fabrication [11], biological and medical sensors [12-13], and two-photon nanostructured semiconductor quantum dots for optical limiters [14-15].

Light has always played a special role in nature with its wave and particle duality. In early history, light was seen as a propagating wave until the photoelectric effect required a particle-like description. With the introduction of quantum mechanics (QM) early in the 20th century, the concept of quantized energy levels became well-known [16]. Energy level diagrams (ELDs) are used in the description of atoms, molecules and ions.

Traditionally, the microscopic interaction of an electromagnetic field and matter was described by a nonlinear system of PDEs, which arose from the QM density matrix formalism [17]. Such systems could seldom be solved exactly and a series of approximations were used to obtain analytical solutions [18]. Later, various numerical algorithms were developed for solving them [19]. However, as lasers became more powerful and pulsed lasers made high intensities possible, even more nonlinear processes have been observed because of occupation of higher energy levels. For example,

[*evp@simphotek.com](mailto:evp@simphotek.com), phone +1 (973) 621-2340; simphotek.com

measurements done with femtosecond (fs) pulse lasers gave rise to intensity levels not observed with nanosecond (ns) or picosecond (ps) pulse lasers, often increasing the number of accessible energy levels (ELs) which need to be included to a mathematical model to achieve a desired level of accuracy in the numerical simulations. Each time a new EL is added to explain higher energy level interactions, more terms and PDEs should be added to the numerical simulation code, which results in a significant time lag in the data analysis process. However, if additions or modifications to the code could be done automatically and in real time, the data analysis would be greatly improved.

In this paper, we define and demonstrate a transition module methodology: a Lego-like system for describing in a uniform way existing and/or composing novel energy level diagrams of, and for building a mathematical model (numerical algorithm) of light interaction with photo-activated materials which is valid for a wide range of multi-photon absorbers and laser regimes. The method uses (computational) transition modules (TMs) or “optical building blocks” describing electronic transitions between different energy levels as well as the levels’ absorption/relaxation parameters that are linked to matrices and vectors in coupled equations of the mathematical model. This approach enables modification so that new energy levels and their corresponding equations with photophysical parameters can be added or deleted without rewriting the numerical algorithm. Combined, they allow one to optimize design functionalities and parameters of a significant variety of photoactive materials, without repeated material synthesis, measurements, or numerical coding.

In a previous paper [20], we introduced and outlined a method to generalize the numerical solutions of laser-matter equations in terms of the light beam intensity and validated it against several examples for single-photon (SPA), two-photon (TPA), and three-photon (3PA) absorbers in solution or solid-state polymers. In particular we validated the numerical algorithm for nanosecond (ns) pulses in AF455 [20] using a five-level ELD model. In this paper we refine the idea of the basic TMs to develop a set of computational TMs for absorption and relaxation and apply it to femtosecond (fs) duration pulses in AF455. We find the increase in intensity gives rise to an experimental regime that cannot be explained by the five-level ELD model used for nanosecond (ns) duration pulses.

2. THEORETICAL METHODS

The energy levels possible for an atom or molecule are described by Schrödinger equations, which describe the quantum states of a physical system. The time-independent Schrödinger equation is used for systems in a stationary state. The ground state, N_0 , initially holds all of the electrons that may be photoexcited to higher ELs. In order to describe the interaction of light and matter, the so-called rate equations can be obtained from the diagonal elements of the density matrix [21,22]. A density matrix describes the statistical state of a quantum system. The density matrix operator is defined as $\hat{g} = |\psi\rangle\langle\psi|$, and the equation of motion is given by [17]

$$\frac{\partial \hat{g}}{\partial t} = \frac{-i}{\hbar} [\hat{H}, \hat{g}], \text{ or } \frac{\partial g_{jk}}{\partial t} = \frac{-i}{\hbar} \sum_l (H_{jl} g_{lk} - g_{kl} H_{lj}), \quad (1)$$

where the matrix elements g_{jk} correspond to a polarization induced by a transition between energy levels j and k . The wave equation of the incident electromagnetic field in the presence of the electric polarization vector is given by Maxwell’s equation in the scalar form

$$\nabla^2 E_x(z, r, t) - \frac{1}{c^2} \frac{\partial^2}{\partial t^2} E_x(z, r, t) = \frac{1}{\epsilon_0 c^2} \frac{\partial^2}{\partial t^2} P_x(z, r, t), \quad (2)$$

where we assume that $\nabla \cdot E = 0$, ϵ_0 is the permittivity and c is the speed of light in vacuum. The x -components of the electric field and its induced nonlinear polarization are given by

$$\begin{aligned} E_x(z, r, t) &= E(z, r, t) \exp[-i(\omega_0 t - k_0 z)] + c.c. \\ P_x(z, r, t) &= P(z, r, t) \exp[-i(\omega_0 t - k_0 z)] + c.c. \end{aligned} \quad (3)$$

where ω_0 and k_0 are the frequency and the wave number of the incident electromagnetic field, and $E(z, r, t)$ and $P(z, r, t)$ are the slowly varying envelopes of the electromagnetic field and the polarization vector, respectively. Assuming that the envelopes are slowly varying along the propagation direction, neglecting the relatively small second derivative of envelope $\partial^2/\partial z^2 E(z, r, t)$ (paraxial approximation), we can rewrite the scalar wave Eq. (2) in the form of the following nonlinear Schrödinger equation

$$\left(\frac{\partial}{\partial z} + \frac{n}{c} \frac{\partial}{\partial t} - \frac{i}{2k_0} \nabla_{\perp}^2 + \frac{\alpha_0}{2} \right) E(z, r, t) = \frac{ik_0}{2\varepsilon_0 n^2} P(z, r, t), \quad (4)$$

where ∇_{\perp}^2 is the Laplacian in the transverse two-dimensional space, such as diffraction, α_0 is linear absorption. The intensity of the light is defined by $I(z, r, t) = 2\varepsilon_0 n c |E(z, r, t)|^2$, where n is the linear index of refraction, and the photon flux at the carrier frequency ω_0 is defined by $\phi(z, r, t) = I(z, r, t) / \hbar \omega_0$. It is convenient to express the electric field slow varying envelope E , defined by Eq.(4), in terms of a normalized function, $Q(\eta, \rho, \tau)$:

$$E(\eta, \rho, \tau) = Q(\eta, \rho, \tau) Q_0, \quad (5)$$

with the following dimensionless parameters $\eta = z/L_{df}$, $\rho = r/R_0$, $\tau = (t - nz/c)/T_0$, where T_0 and R_0 are the 1/e pulse width and beam radius, respectively, $L_{df} = k_0 R_0^2/2$ is the diffraction length, λ_0 is the beam wavelength, and c is the speed of light in vacuum. The propagation Eq. (4) can be written in the new coordinates as follows

$$\frac{dQ(\eta, \rho, \tau)}{d\eta} = \frac{1}{2} \left\{ -L_{df} N_T \left[\sum_{m=1}^{M_T} (\mathbf{d}_m \cdot \mathbf{N}(\eta, \rho, \tau)) I_0^{m-1} |Q|^{2(m-1)}(\eta, \rho, \tau) \right] - \alpha_0 L_{df} \right\} Q(\eta, \rho, \tau), \quad (6)$$

after the diffraction term (given by the Laplacian ∇_{\perp}^2) is excluded. The imaginary part of nonlinear polarization envelope $P(z, r, t)$ contributes absorption terms in the form of $-\sigma_{ij}^{[m]} N_i(\eta, \rho, \tau) N_T (2\varepsilon_0 n c Q_0^2)^{m-1} |Q(\eta, \rho, \tau)|^{2(m-1)} Q(\eta, \rho, \tau)$ to Eq. (6). Each decreases the normalized field Q due to simultaneous absorption of m photons by atoms or molecules being in i^{th} energy state [concentration of which is given by $N_i(\eta, \rho, \tau)$, and $N_T = \sum_i N_i(\eta, \rho, \tau)$ is constant of the total concentration]. Such terms can be grouped according to the numbers of photons, which allows us to write the propagation equation in a more compact form by using vectors of absorption coefficients \mathbf{d}_m and the vector of normalized population densities of atoms or molecules at chosen energy states $\mathbf{N} = (N_0, \dots, N_{s-1})$. The real part of polarization is also excluded (e.g., such part forms a Kerr term among others). The derivation of the electromagnetic field including diffraction and the Kerr effect is given in refs. [22] and [23]. The rate equations, derived from Eq. (1), see ref. [21] can also be generalized in the similar way by grouping terms with the same number of absorbed photons. It can be written in terms of normalized envelope $Q(\eta, \rho, \tau)$ in a more compact form:

$$\frac{\partial \mathbf{N}(\eta, \rho, \tau)}{\partial \tau} = T_0 \left[\mathbf{D}_0 + \sum_{m=1}^{M_T} \frac{\mathbf{D}_m I_0^m}{m \hbar \omega_0} |Q|^{2m}(\eta, \rho, \tau) \right] \mathbf{N}(\eta, \rho, \tau). \quad (7)$$

Equations (6) and (7) form the coupled equations used in this paper, and have the following definitions: \mathbf{D}_m are constant $S \times S$ matrices of decay rates k_{ij} for $\mathbf{D}_0 (\{k_{ij}\})$, and molar absorption cross-sections $\sigma_{ij}^{[m]}$ for $\mathbf{D}_m (\{\sigma_{ij}^{[m]}\})$ when $m > 0$ photons are absorbed, $\mathbf{d}_m (\{\sigma_{ij}^{[m]}\})$ are constant S -dimensional vectors, and $I_0 = 2\varepsilon_0 n c Q_0^2$ is the peak intensity, where Q_0 is electric field strength given in units of V/m.

3. ABSORPTION AND RELAXATION TRANSITION MODULES

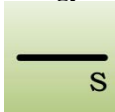
In our approach (computational) transition modules (TMs) describe all the segments of energy level diagram (ELD), where each segment defines an entity (e.g., electron) transitioning between two energy levels (ELs). It is very useful to classify the ELs by relating them to some quantum number, p . As an example, we use an EL classification based on the total angular momentum, $M(s) = 2J + 1$, $J=0,1,\dots$; however, we do not impose any restrictions on the basis of classification. We group ELs of the same quantum number into q-sets given by ${}^pM = \{s \mid M(s) = p\}$. For example, the singlet states – the states with the spin multiplicity $M=1$ – will be denoted by 1M , the triplet states with the spin multiplicity $M=3$ will be denoted by 3M .

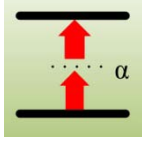
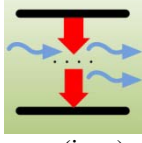
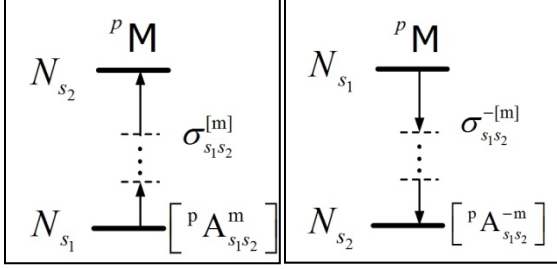
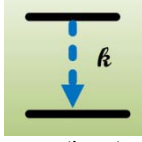
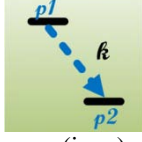
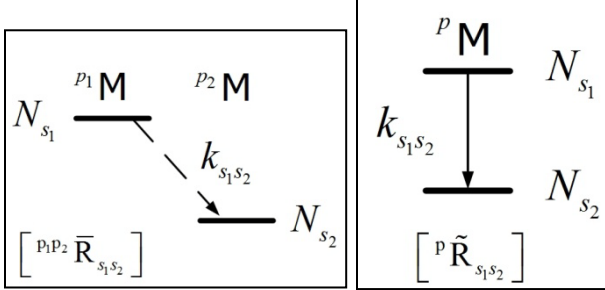
We distinguish two types of TMs: absorption transition modules and relaxation transition modules as described in Table 1.

1. The *absorption module*, denoted by ${}^pA_{s_1s_2}^{[m]}$, represents a numerical model of simultaneously absorbing m photons by an entity (e.g., electron) and dislocating such entity from one EL s_1 to another EL s_2 within the same q-set pM . We distinguish the two types of photon absorption model. The first type is the *forward absorption*, $\alpha > 0$, [Table 1] during which a photoactivated entity is promoted from a lower EL to a higher EL. According to the second type of the absorption mechanism [Table 1], an entity relaxes from a higher EL to a lower EL by re-emitting photons coherent with the incident light. In this case we assume that $\alpha < 0$ and label it the *inverse absorption* (e.g., stimulated emission). The indices of the absorption block ${}^pA_{s_1s_2}^{[m]}$ are p , m , s_1 , and s_2 ; whereas, $\sigma_{s_1s_2}^{[m]}$ is a parameter of the absorption block. We combine all absorption blocks in one large group $A = \left\{ {}^pA_{s_1s_2}^{[m]} \mid \alpha \in \mathbb{Z} \setminus \{0\}, \text{ and } s_1s_2, p \text{ are all in } \mathbb{N}_0 \right\}$.

The second type of our computational TM is a *relaxation module*, denoted by ${}^{p_1p_2}_{s_1s_2} \overset{\text{type}}{R}$, which represents the entity's relaxations between the states of the same or different q-sets. In its general description, a relaxation module represents an event of an entity migration from a higher EL $s_1 \in {}^{p_1}M$ to a lower EL $s_2 \in {}^{p_2}M$, by either emitting radiation (and, in this case, the event is the radiative transfer specified by wave sign: type = '~' in the diagram expression) or by non-radiative (e.g., heat) relaxation (specified by a bar: type = '-'). If the relaxation mechanism is not known, then the type is left blank. The relaxation module has a parameter $k_{s_1s_2}$ of the relaxation decay rate. Examples of derived blocks corresponding to different relaxation scenarios are shown in Table 1, where ${}^{p_1p_2}_{s_1s_2} \bar{R}$ is a relaxation module of non-radiative migration of electron parameterized by intersystem crossing decay rate $k_{s_1s_2}$, and in Table 1, where ${}^p\tilde{R}_{s_1s_2}$ is a relaxation module corresponding to emission during migration of an electron within the states of the same spin multiplicity p . We also group all possible relaxation TMs in a separate set of relaxation blocks $R = \left\{ {}^{p_1p_2}_{s_1s_2} \overset{t}{R} \mid t \in \{ '~', '- ', ' ' \}, \text{ and } s_1s_2, p_1, p_2 \text{ are all in } \mathbb{N}_0 \right\}$. A *generic photoactive material* can be related to its *transitions string* χ , which is a union of TM expressions from the set $A \cup R$. For example, a transition string $\chi_{AF455(ns)} = {}^1A_{01}^{[2]} \cup {}^1A_{12}^{[1]} \cup {}^3A_{34}^{[1]} \cup {}^1\tilde{R}_{10} \cup {}^1R_{21} \cup {}^3R_{43} \cup {}^{13}\bar{R}_{13} \cup {}^{31}\tilde{R}_{30}$ represents the two photon absorbing (TPA) chromophore AF455.

Table 1. The transition modules for absorption and relaxation and their corresponding descriptions.

Transition Modules	Description and Parameters
Energy Level 	Unified (computational) energy level. It may represent electronic level, vibrational level, rotational level, continuum level, combination of degenerate levels, hypothetically added level with the condition that it makes a significant contribution to the macroscopic physical phenomena.

<p>Absorption Transition Module</p>  <p>(icon)</p>  <p>(icon)</p>	<p>Absorption TM represents single-/multi- photon absorption or stimulated emission. Below are the absorption block diagram and parameters.</p>  <p>s_1, s_2 indices of the energy levels the electrons are promoted (or relaxed, for stimulated emission) “from” and “to”;</p> <p>m a number of simultaneously absorbed (or inverse absorbed, for simulated emission) photons;</p> <p>p index of the q-set, to which the source and the destination levels belong to;</p> <p>$\sigma_{s_1 s_2}^{[m]}$ absorption molar cross-section;</p> <p>$\sigma_{s_2 s_1}^{-[m]}$ simulation emission cross-section;</p>
<p>Relaxation Transition Module</p>  <p>(icon)</p>  <p>(icon)</p>	<p>Relaxation transition module represents electron/exciton relaxation happening between the states of the same or different q-sets.</p>  <p>TM parameters are</p> <p>s_1, s_2 indices of the energy levels the electrons relax “from” and “to”;</p> <p>type type = '~' is radiative transfer, and type = '-' is non-radiative transfer;</p> <p>p_1, p_2 indices of the q-sets for the source and the destination electronic levels;</p> <p>$k_{s_1 s_2}$ relaxation decay rate;</p>

Our TMs are in a way similar to computational molecules: they uniquely define corresponding terms in the coupled system of rate-propagation Eqs. (6) and (7). For a given transition string $\chi = \cup_i e_i$, we start with zero matrices D_0, D_1, \dots and zero vectors d_0, d_1, \dots and for each e_i we update the matrices and vectors as follows:

(1) if $e_i = {}^p A_{s_1 s_2}^{[m]}$, with the absorption parameter $\sigma_{s_1 s_2}^{[m]}$ we perform

$$D_{|m|}[s_1, s_1] = D_{|m|}[s_1, s_1] - \sigma_{s_1 s_2}^{[m]},$$

$$D_{|m|}[s_2, s_1] = D_{|m|}[s_2, s_1] + \sigma_{s_1 s_2}^{[m]}, \quad (8)$$

$$\sigma_{|m|}[s_1] = \sigma_{|m|}[s_1] + \text{sgn}(m) \sigma_{s_1 s_2}^{[m]};$$

(2) if $e = \overset{t}{p_1 p_2} R_{s_1 s_2}$, with decay rate $k_{s_1 s_2}$; we update

$$D_0[s_1, s_1] = D_0[s_1, s_1] - k_{s_1 s_2},$$

$$D_0[s_2, s_1] = D_0[s_2, s_1] + k_{s_1 s_2}. \quad (9)$$

4. APPLICATION TO AN ORGANIC CHROMOPHORE

4.1. Absorption parameters

Energy level diagram (ELD) description is a key parameter in our simulation algorithm. Exemplary analysis of nonlinear behavior of AF455 chromophore is based on an ELD which is obtained from published spectroscopic data [24]. The absorption (Fig. 1a), fluorescence (Fig. 1c), and phosphorescence (Fig. 1d) spectra of the singlet states of AF455 are shown as reconstructed from the data in ref. [24]. Fig. 1(b) shows the triplet absorption from ref. [24]. Figs. 1(a), 1(b) and 1(c) are at room temperature; while Fig. 1(d) is at 77K. Fig. 1(b) is the transient spectrum obtained after 355 nm excitation and the molar absorption was determined by a singlet depletion method [24].

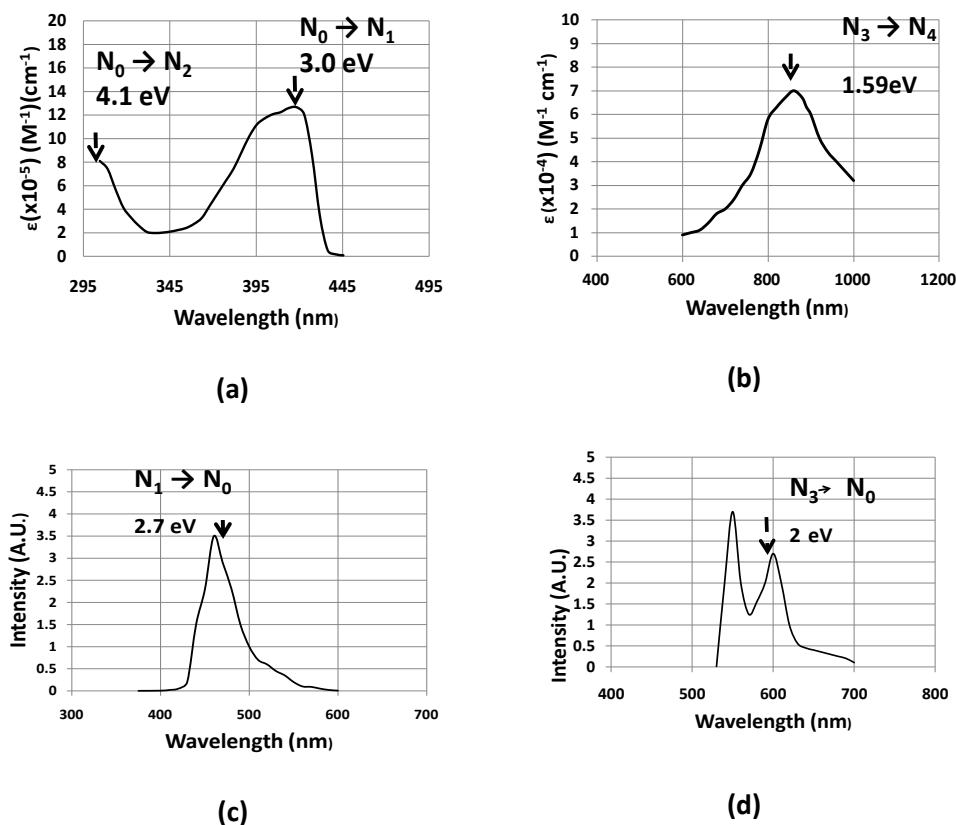


Fig. 1. Spectra of AF455 taken from ref. [24]. (a) Absorption spectrum of the singlet states, (b) Absorption spectrum of triplet states, (c) emission spectrum from first excited state to ground state within the singlet manifold, (d) emission spectrum from excited state to ground state within the triplet manifold.

Fig. 2 shows the ELD for AF455 in the spectral region of interest. Fig. 2(a) shows a brief schematic diagram with the three singlet energy levels and the two triplet energy levels. The values for the five energy levels have been obtained

from the peaks and sudden spikes in the spectral measurement in Fig. 1. In general, the electronic energy levels are broadened by vibrations, but only a few of these levels are shown by dashed horizontal lines, for simplicity. Electrons promoted to vibrational energy levels within an electronic state manifold decay much faster than the electronic states and, in general, are not considered in the mathematical equations. However, the vibrational energy levels can be included in our methodology if needed. Fig. 2(b) shows a simplified ELD corresponding to Fig. 2(a) in which all vibrational energy levels are neglected.

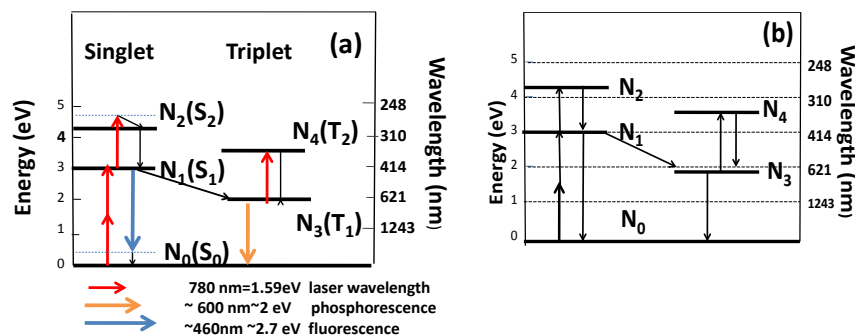


Fig. 2. Energy level diagrams of five-level AF455 as functions of energy (eV) and wavelength (nm). (a) Schematic diagram with laser absorptions shown in red, fluorescence in blue and phosphorescence in gold. (b) Simplified (a) in with transitions in black.

Our original mathematical algorithm was extensively tested and validated on a number of five level multi-photon absorbers at relatively low ns laser intensity transmission experiments in our earlier work [20]. As the laser pulse width decreases the intensity of the beam increases for a given input energy. In such cases additional ELs may be populated that were not populated at lower light intensities. In transmission experiments this may appear when the transmission curve shows more absorption at high intensity than the initial model predicts. In such a case one may postulate that the additional absorption at high intensities is due to the population of additional EL(s) in the material. But, introducing additional photoactivated absorption and relaxation processes requires several new equations added to the coupled rate equations, i.e. Eqs. (6) and (7). Because this new set of coupled equations must be solved numerically, traditional numerical software needs to be rewritten or modified. This process can take considerable time and result in several postulates that must be verified by experimental data. We show that this time consuming process can be accomplished in near real-time using the TM algorithms presented here. In the following example, we apply our TMs framework to describe a commonly used five-level model of AF455 for low intensity laser beams and demonstrate how to modify it to a new six-level model, which reveals better agreement with transmittance measurements at high input laser intensity. This well-known experimental method measures the laser beam energy before and after transmission through a sample material. The ratio of the light energy is calculated and plotted as a function of incident laser energy/intensity. Numerical analysis of the experimental data can provide information about the photophysical parameters and accessible, i.e. populated ELs.

4.2 Experimental Method

Measurements of AF455 (Fig. 3) were taken with a 175 fs (sech^2 FWHM), $\lambda_0=780\text{nm}$, plane-polarized light pulses from Ti:S regenerative amplifier (Clark-MXR CPA-2010) which were focused with a 750mm lens into a 5.1mm thick PMMA slab doped with TPA chromophore AF-455 at a concentration of $1.85 \times 10^{18} \text{ cm}^{-3}$, and index of refraction, $n=1.4$. The front face of the sample was positioned at the focal plane of the lens. The energy of the pulses was varied using a variable attenuator consisting of a rotatable waveplate ($\lambda/2$) and fixed polarizer. The range of input energies (intensities) in this experiment was $0.01 \mu\text{J}$ (0.97 GW/cm^2) to $25 \mu\text{J}$ ($2.4 \times 10^3 \text{ GW/cm}^2$). Pulse energies were measured before and after the sample and the ratio of transmitted to incident pulse energy computed. The ratio η of the sample length to the diffraction length is $\eta = z/L_{df} = 0.57$, $L_{df} = \pi R_0^2 n / \lambda_0$. Because this ratio is less than one, diffraction does not occur in this sample. This justifies validity of using the simplified model of light propagation given by Eq. (6). The insert in Fig. 3 shows the transmission data at energies above $2 \mu\text{J}$. Data are courtesy of the Air Force Research Laboratory, Wright-Patterson Air Force Base, Ohio.

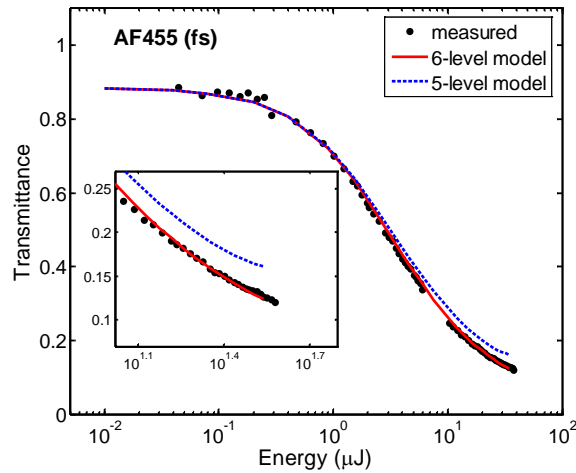


Fig. 3. AF455 transmission measurements as a function of input light energy. The experimental data (AFRL, Write-Patterson) are shown by black dots, the blue dashed line is our calculation using a five-level model, and the red solid line is our calculation using a six-level model. The insert shows a magnification of the right-hand tail of the figure.

In Fig. 3 the data points are shown as black dots. We calculated transmittance (T_E , given below) of the laser light through the sample of AF455 by solving the system of Eqs. (6) and (7) for the five-level model (given by the dashed line) and for the new six-level model (given by the solid line).

$$T_E = \frac{E_{out}}{E_{in}} = \frac{\int_0^{+\infty} d\rho' \int_{-\infty}^{+\infty} d\tau' |Q(\eta_{max}, \rho', \tau')|^2}{2\pi \int_0^{+\infty} d\rho' \int_{-\infty}^{+\infty} d\tau' Q_0^2 \sec^2 h^2(\tau') e^{-(\rho')^2}}. \quad (10)$$

Table 2 gives the absorption parameters for the experiments and the single photon absorptions. Other experimental parameters are the relaxation rates $k_{10}^{-1}, k_{21}^{-1}, k_{31}^{-1}, k_{30}^{-1}, k_{43}^{-1}, k_{52}^{-1} = 2.72\text{ns}, 1.66\text{ps}, 45.3\text{ns}, 368\text{ms}, 10\text{ns}, 160\text{fs}$, respectively; and $z_{max}, N_T, R_0, T_0, \lambda_0 = 5.1\text{mm}, 1.85 \times 10^{-3}\text{nm}^{-3}, 40.57\mu\text{m}, 99.95\text{fs}, 780\text{nm}$, respectively.

Table 2. Left shaded side: Absorption parameters for the AF455 chromophore. Right unshaded side: Values of absorption cross-sections and molar extinction coefficients for single-photon absorptions.

Experimental Parameter	AF455 ^a Value	Absorption Cross Section	Value	Molar Extinction Coefficient	Value	Wave-length
$\sigma_{01}^{[2]} (\text{cm}^2/\text{GW})$	0.5×10^{-20}	SINGLE PHOTON ABSORPTIONS (SINGLET STATES)				
$\sigma_{12}^{[1]} (\text{cm}^2)$	1.68×10^{-17}	$\sigma_{01}^{[1]} (\text{cm}^2)$	5.74×10^{-15}	$\epsilon^b (\text{M}^{-1}\text{cm}^{-1})$	15×10^5	414(nm)
$\sigma_{34}^{[1]} (\text{cm}^2)$	17.1×10^{-17}	$\sigma_{02}^{[1]} (\text{cm}^2)$	3.06×10^{-15}	$\epsilon^b (\text{M}^{-1}\text{cm}^{-1})$	8×10^5	303(nm)
$\sigma_{25}^{[1]} (\text{cm}^2)$	0.78×10^{-17}	$\sigma_{05}^{[1]} (\text{cm}^2)$	$< 3 \times 10^{-15}$	$\epsilon^c (\text{M}^{-1}\text{cm}^{-1})$	$< 8 \times 10^5$	214(nm)

a refs. [20], [24] and [25].

b ref [24].

c estimated value, this paper.

The blue dashed line in Fig. 3 shows a good fit of the five-level model to the measurements in the range from about 0.01 μJ (0.97 GW/cm^2) to about 2 μJ ($1.94 \times 10^2 \text{ GW/cm}^2$) using the parameters in Table 2. However, we can see that at energies exceeding about 2 μJ the calculations diverge from the experimental data. Given the high intensity in this region (Fig. 3), it is reasonable to expect electrons to be promoted to higher EL

4.3 Investigating an additional electronic level.

Next, we investigate possibilities that could account for the higher absorption observed above 2 μJ . In order to understand the experimental data, we postulate an additional accessible EL. The chromophore has both singlet and triplet electronic states. In order to distinguish between additional singlet or triplet states, we calculate the population dynamics, at 2 μJ as shown in Fig. 4(a) and find that the electrons populate the singlet states N_1 and N_2 ; whereas, the triplet states N_3 and N_4 are not significantly populated. Fig. 4(b) shows the normalized absorption i.e. the exact contributions from each electronic level to the total absorption (refer to Eq. (28) in [20]). It confirms that the absorption is due to a combination of absorptions from the ground state to the first (due to the leading part of the pulse) and second excited states of the singlet manifold (due to the trailing edge of the pulse).

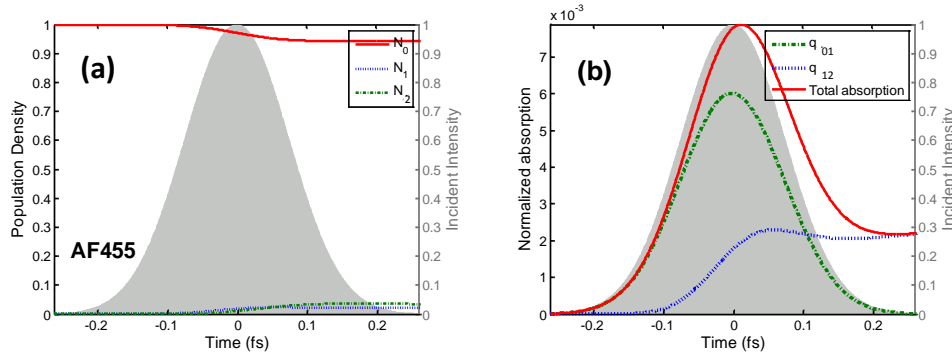


Fig. 4. AF455 five-level model, input energy 2 μJ . (a) Population density as a function of temporal pulse width for three electronic states, N_0 , N_1 and N_2 . The grey shadow area represents the normalized intensity of the femtosecond light pulse. (b) Normalized absorption as a function of the temporal pulse width for total absorption (solid line), the absorptions from N_0 to N_1 (q_{01} -dash-dot line) and N_1 to N_2 (q_{12} -dotted line). The grey shadow area represents the normalized intensity of the femtosecond light pulse.

Therefore, we “postulate” a higher energy singlet state resulting in a six-level model as shown in Fig. 5 where the dashed red oval encircles the additional singlet state and new transitions. This will translate to adding two new TMs to the transitions string $\chi'_{\text{AF455}} = \chi_{\text{AF455}} \cup {}^1\text{A}_{25}^{[1]} \cup {}^1\text{R}_{52}^{[1]}$, within $\text{A} \cup \text{R}$ framework. The updated set of coupled rate equations is given by (for brevity, we write the rate equations in terms of the intensity in the original variables)

$$\begin{aligned}
 \partial N_0 / \partial t &= -(\sigma_{01}^{[2]} I^2 / 2\hbar\omega_0) N_0 + k_{10} N_1 + k_{30} N_3 \\
 \partial N_1 / \partial t &= (\sigma_{01}^{[2]} I^2 / 2\hbar\omega_0) N_0 - (\sigma_{12}^{[1]} I / \hbar\omega_0) N_1 - k_{13} N_1 - k_{10} N_1 + k_{21} N_2 \\
 \partial N_2 / \partial t &= (\sigma_{12}^{[1]} I / \hbar\omega_0) N_1 - k_{21} N_2 - (\sigma_{25}^{[1]} I / \hbar\omega_0) N_2 + k_{52} N_5 \\
 \partial N_3 / \partial t &= k_{13} N_1 - (\sigma_{34}^{[1]} I / \hbar\omega_0) N_3 - k_{30} N_3 + k_{43} N_4 \\
 \partial N_4 / \partial t &= (\sigma_{34}^{[1]} I / \hbar\omega_0) N_3 - k_{43} N_4 \\
 \partial N_5 / \partial t &= (\sigma_{25}^{[1]} I / \hbar\omega_0) N_2 - k_{52} N_5
 \end{aligned} \tag{11}$$

The additional level adds/modifies at least two rate equations, which traditionally requires modification to the numerical algorithm and leads to down time for writing software modifications. In our TM approach, the numerical algorithm remains unchanged [20,23] – we only update vectors and matrices according to Eqs. (8) and (9). A diagram with TM icons, shown on the right portion in Fig. 5, demonstrates what is required to update the underlying numerical solver without changing the code and working only in some graphical user interface (GUI). Each new TM icon will correspond to the corresponding terms in the rate and propagation equations (e.g., this correspondence is shown for the rate equations on the bottom left portion in Fig. 5). Therefore, GUI with a set of our TM icons defines ELD of the material and automatically builds the rate and propagation equations. In our example, the set of TM icons in Fig. 5 will translate

to the set of Eqs. (11). The figure helps to show the flow of the algorithm, while the details of the figure are given in the respectively noted sections of the paper.

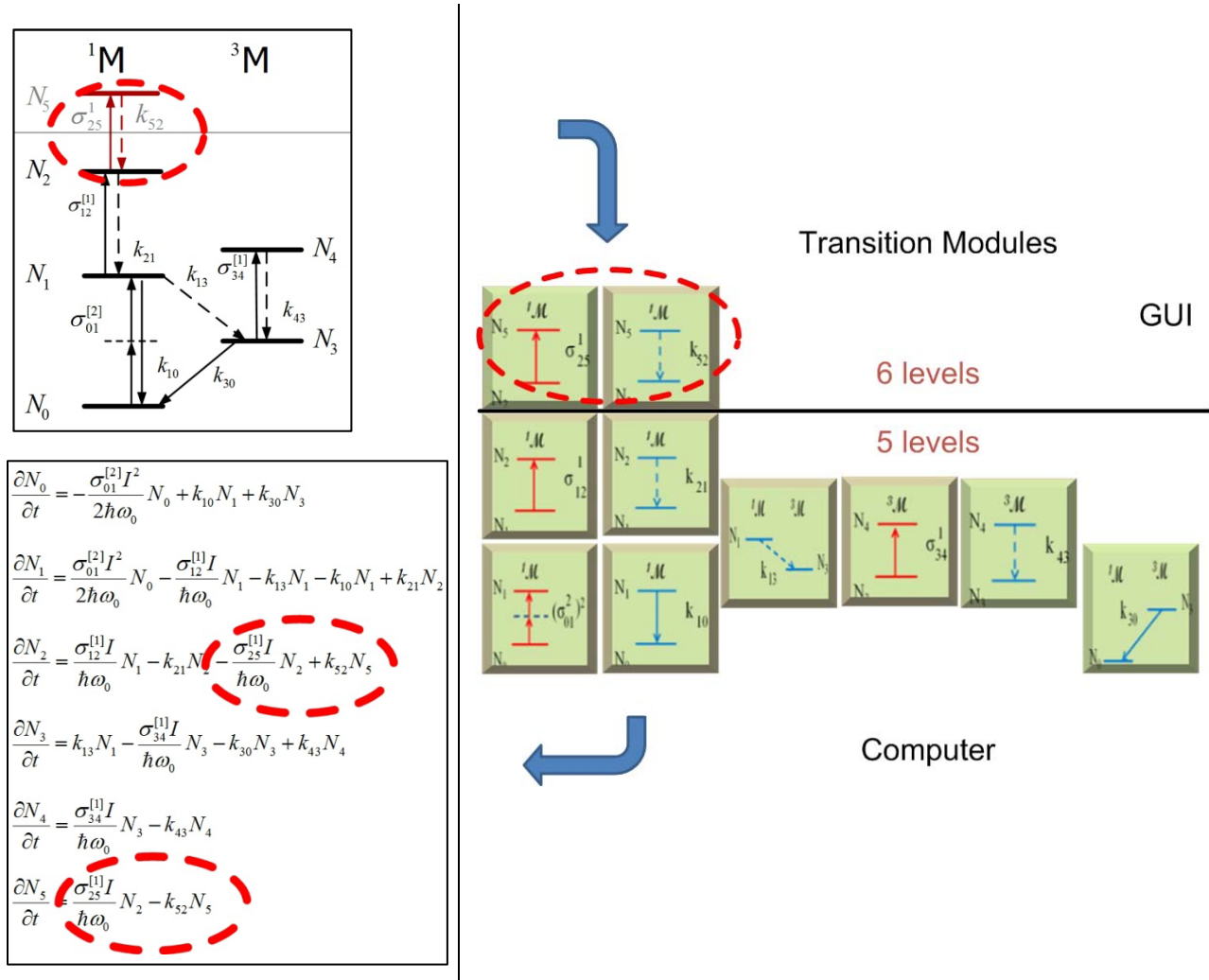
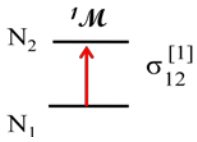
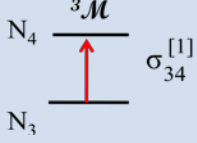
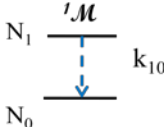
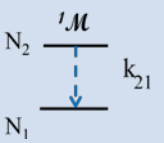
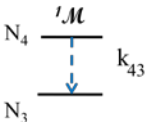
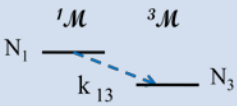
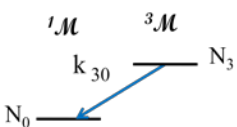
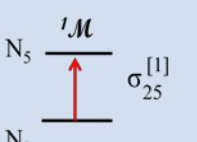
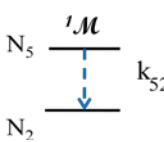


Fig. 5. Schematic diagram of the flow of the Transition Module (TM) algorithm. Upper left section is a new 6-level energy level diagram, the section on the right is a composite of TM icons from Table 1, and the lower left section is a miniature of Eq. (11) with encircled terms corresponding to encircled icons.

Table 3 shows the TM diagrams and their corresponding partial equations associated with each one as determined by our algorithm. While the propagation equation is also modified by the TMs, only the modified rate equations are shown in the Fig. 5 and Table 3, for simplicity. The TM diagram is a computational diagram used to visualize the collection of TMs (See Table 3.) used by our algorithm to solve Eqs. (6) and (7).

Table 3. Diagram expressions, transition modules and equation fragments used for the AF455 six-level model.

Expression	Transition Module	Equation fragments
$1A_{01}^{[2]}$		$\frac{\partial N_0}{\partial \tau} = \dots - \frac{\sigma_{01}^{[2]} I_0^2}{2\hbar\omega_0} Q ^4 T_0 N_0 + \dots$ $\frac{\partial N_1}{\partial \tau} = \dots + \frac{\sigma_{01}^{[2]} I_0^2}{2\hbar\omega_0} Q ^4 T_0 N_0 + \dots$

${}^1A_{12}^{[1]}$		$\frac{\partial N_2}{\partial \tau} = \dots + \frac{\sigma_{12}^{[1]} I_0}{\hbar \omega_0} Q ^2 T_0 N_1 + \dots$ $\frac{\partial N_1}{\partial \tau} = \dots - \frac{\sigma_{12}^{[1]} I_0}{\hbar \omega_0} Q ^2 T_0 N_1 + \dots$
${}^3A_{34}^{[1]}$		$\frac{\partial N_3}{\partial \tau} = \dots - \frac{\sigma_{34}^{[1]} I_0}{\hbar \omega_0} Q ^2 T_0 N_3 + \dots$ $\frac{\partial N_4}{\partial \tau} = \dots + \frac{\sigma_{34}^{[1]} I_0}{\hbar \omega_0} Q ^2 T_0 N_3 + \dots$
${}^1\tilde{R}_{10}$		$\frac{\partial N_1}{\partial \tau} = \dots - k_{10} T_0 N_1 + \dots$ $\frac{\partial N_0}{\partial \tau} = \dots + k_{10} T_0 N_1 + \dots$
${}^1R_{21}$		$\frac{\partial N_2}{\partial \tau} = \dots - k_{21} T_0 N_2 + \dots$ $\frac{\partial N_1}{\partial \tau} = \dots + k_{21} T_0 N_2 + \dots$
${}^3R_{43}$		$\frac{\partial N_4}{\partial \tau} = \dots - k_{43} T_0 N_4 + \dots$ $\frac{\partial N_3}{\partial \tau} = \dots + k_{43} T_0 N_4 + \dots$
${}^{13}\bar{R}_{13}$		$\frac{\partial N_3}{\partial \tau} = \dots + k_{13} T_0 N_1 + \dots$ $\frac{\partial N_1}{\partial \tau} = \dots - k_{13} T_0 N_1 + \dots$
${}^{31}\tilde{R}_{30}$		$\frac{\partial N_3}{\partial \tau} = \dots - k_{30} T_0 N_3 + \dots$ $\frac{\partial N_0}{\partial \tau} = \dots + k_{30} T_0 N_3 + \dots$
${}^1A_{25}^{[1]}$		$\frac{\partial N_5}{\partial \tau} = \dots + \frac{\sigma_{25}^{[1]} I_0}{\hbar \omega_0} Q ^2 T_0 N_2 + \dots$ $\frac{\partial N_2}{\partial \tau} = \dots - \frac{\sigma_{25}^{[1]} I_0}{\hbar \omega_0} Q ^2 T_0 N_2 + \dots$
${}^1R_{52}$		$\frac{\partial N_5}{\partial \tau} = \dots - k_{52} T_0 N_5 + \dots$ $\frac{\partial N_2}{\partial \tau} = \dots + k_{52} T_0 N_5 + \dots$

4.4 Optimization

We have introduced two parameters k_{s2}^{-1} (relaxation time from level 5 to level 2) and $\sigma_{25}^{[1]}$ (absorption coefficient from level 2 to level 5). We use the following optimization procedure to fit these parameters to the experimental data presented in Fig. 3. Fitting a physical parameter p to the transmission measurements is done by optimizing some objective function $F(p)$ of a general least squares form $F(p) = \sum_{j=1:M} (h(p; t_j) - y_j)^2$, where y_j are the measured (observed) values and $h(p; t_j)$ are the corresponding values calculated by a model function. In contrast to most of the existing fitting frameworks, the model function is not given by a close formula approximation, but rather based on a numerical solution of complete propagation model, given by coupled PDEs (6) and (7). A broad set of parameters is available for fitting in our optimizer, $p \in \Sigma = \Sigma_{MPA} \cup \Sigma_K \cup \Sigma_N \cup \Sigma_{EMF} \cup \Sigma_{SMP}$. It contains the photophysical parameters for a given material, such as the multi-photon absorption cross-sections, $\Sigma_{MPA} = \{\sigma_{ij}^{[2]}, \sigma_{ij'}^{[3]}, \dots, \sigma_{ij''}^{[m]}, \dots\}$, the single photon absorption cross-sections, $\Sigma_{SPA} = \{\sigma_{ij}\}$, the relaxation rates, $\Sigma_K = \{k_{ij}\}_{ij}$, and the index of refraction, $\Sigma_N = \{n\}$, some parameters describing the laser beam, $\Sigma_{EMF} = \{T_0, R_0\}$, and terms describing the sample, $\Sigma_{SMP} = \{L, T_{Fresn}, N_\tau\}$. All other parameters, call it Π , including the computational grid sizes, pulse shape and frequency, are fixed for the transmission experiment except the input energy E_{in} , which changes according to the experimental data: $t_j = E_{in}[j]$ is the incident energy value E_{in} in j^{th} experiment ($j=1 \dots M$). The rest of the optimization values are set as follows: $y_j = T_E^e[j]$ is the measured transmission value T_E in j^{th} experiment, and model function $h(p; E_{in}) = T_E(p; Q^{(s)}(p; E_{in}))$ returns the transmission values given by Eq. (10), which are calculated numerically by solving Eqs. (6) and (7) using our version of split-step numerical scheme [20,23].

The high-level description of the optimization algorithm consists of two main functional blocks (“optimizer” and “numerical solver”), fixed input, varying input, and data interfaces. The optimizer block sequentially finds the next trial optimal value p_{k+1} based on the previous parameter values $\{p_{k'}\}_{k'=1:k}$ and the weighted difference between the measured transmission values $\{y_j\}_{j=1:M}$ and calculated transmission values $\{h_{kj} = h(p_k, E_{in}[j])\}_{j=1:M}$. The numerical solver block numerically solves coupled PDEs (6) and (7) to calculate the transmission values h_{kj} . The optimizer block is initialized with an initial guess p_0 and the set of observed values, $\{y_j\}_{j=1:M}$, while the numerical solver is initialized with the corresponding sample values, $\{t_j\}_{j=1:M}$, which were used during the experiments, and with the values for all the fixed parameters $(\Sigma \setminus p) \cup (\Pi \setminus E_{in})$. Though computationally more expensive, our optimizer achieves better accuracy for target fitting parameters, which could be the only choice in cases when conventional approximations break.

4.5. Analysis of Experimental Data

Initial results from quantum calculations by Artem Masunov [26] have indicated the presence of N_5 level. Using our optimization procedure, we obtain the parameters $k_{s2}^{-1} = 160$ fs and $\sigma_{25}^{[1]} = 0.78 \times 10^{-17}$ cm². These parameters are realistic as the absorption from N_2 to N_5 is expected to be less than that of the absorption from N_1 to N_2 and relaxation from higher levels is usually in the fs range [24-25]. The red curve in Fig. 3 is calculated with the resulting AF455 six-level model and shows excellent agreement with the experiment. For completeness, we calculate the population densities along the center of the pulse ($\rho=0$) and normalized absorption at 20 μ J in Fig. 6. Fig. 6(a) shows the population densities as a function of time. All levels (N_0 - N_5) were included in the calculation, but only the singlet levels N_0 , N_1 , N_2 , and N_5 show appreciable changes. As expected, the two triplet states, N_3 and N_4 do not show any measurable population densities. As can be seen from Fig. 6(a), the ground state level N_0 is depleted by the leading edge of the pulse and level N_5 achieves

the largest population near the center of the pulse. Level N_1 retains modest population as electrons are excited to N_2 and N_5 . At the trailing edge of the pulse, the electrons are cycled between levels N_2 and N_5 even after the pulse has passed through the distance element of the material. Fig. 6(b) shows the normalized absorption, as defined in ref. [20], which agrees with Fig. 6(a). At the leading edge of the pulse most of the absorption comes from the N_0 to N_1 transition (i.e. q_{01}), while at the trailing edge most of the absorption comes from the N_2 to N_5 transition (i.e. q_{25}).

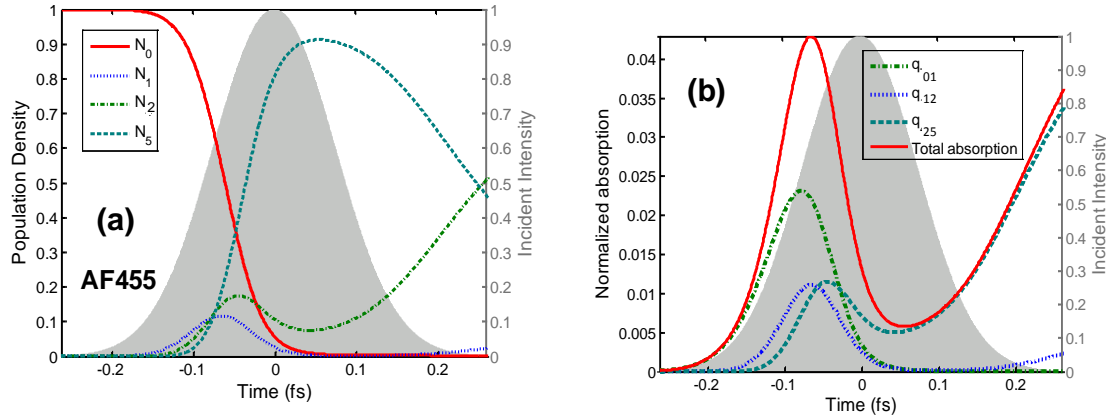


Fig. 6. AF455 six-level model, input energy 20 μ J. (a) Population density as a function of temporal pulse width for four electronic states, N_0 , N_1 , N_2 and N_5 . (b) Normalized absorption as a function of the temporal pulse width for the total absorption (solid line), the absorptions from N_0 to N_1 (q_{01} -dash-dot line), N_1 to N_2 (q_{12} -dotted line) and N_2 to N_5 (q_{25} -dashed line). The grey shadow areas represent the normalized intensity of the femtosecond light pulse.

Knowing the energy of the absorbed photon (780 nm), we can calculate the single photon absorption for this energy level. Fig. 7 shows the single photon absorptions in question as broken arrows, while the rest transitions are shown as solid arrows. For example, the absorption due to the sixth-level (N_0 to N_5) would appear at energy (wavelength) of about 5.8eV (214nm) as shown in Fig.7 by the purple arrow (dashed line). The relationship between the absorption cross-section and the molar extinction coefficient is given by $\sigma(\text{cm}^2) = 10^3 \ln(10) \epsilon(\text{M}^{-1} \text{cm}^{-1}) / N_A = 3.82 \times 10^{-21} \epsilon(\text{M}^{-1} \text{cm}^{-1})$ where $N_A = 6.022 \times 10^{23} (\text{M} / \text{L})$. Using this expression we give the absorption cross sections and the molar extinction coefficients for the single photon absorptions in Table 2. The exact molar extinction coefficient for the transition N_0 to N_5 is unknown, but we can estimate that it is less than $8 \text{ M}^{-1} \text{cm}^{-1}$ because we assume that it will be less than that of the lower energy transition, i.e. N_0 to N_2 .

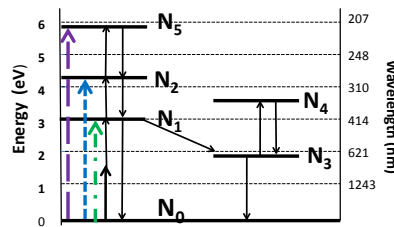


Fig. 7. Six-level diagram with multi-photon absorption shown by solid lines, single photon transitions from N_0 to N_1 (dot-dashed line), N_0 to N_2 (dotted line), and N_0 to N_5 (dashed line).

5. Conclusions

In summary, we have described a novel numerical framework of computational transition modules (TMs), which encodes the EL diagram of a generic photoactive material into a union of generalized computational TMs whose symbolic representations uniquely define terms in a set of rate-propagation equations. It allows investigating a plane electromagnetic wave propagating through generic organic or inorganic photoactive materials while ELs and photo-transitions are implemented without rewriting its numerical code.

Acknowledgment

This work was supported in part by the Air Force Office of Scientific Research. We thank D. Pikas, G.L DesAutels, and M. Walker of the Air Force Research Laboratory Materials and Manufacturing Directorate for supplying the experimental data in Fig. 3. We also thank Artem Masunov of University of Central Florida for initial quantum calculations of AF455.

REFERENCES

- [1] Koos, C. , Jacome , L., Poulton, C., Leuthold , J. and W. Freude, "Nonlinear silicon-on insulator waveguides for all-optical signal processing," *Opt. Express* **15**, 5976–5990 (2007).
- [2] Gratzel, M., "Solar energy conversion by dye-sensitized photovoltaic cells," *Inorg. Chem.* **44**, 6841-6851 (2005).
- [3] Chung, W., Park, K., Jeong Yu, H., Kim, J., Chun, B.-H., Kim, S. H., "White emission using mixtures of CdSe quantum dots and PMMA as a phosphor," *Opt. Mat.* **32**, 515-521 (2010).
- [4] Yoo, H. S., Im, W. B., Kang, J. H., Jeon, D. Y., "Preparation and photoluminescence properties of $\text{YAl}_3(\text{BO}_3)_4\text{:Tb}^{3+}$, Bi^{3+} phosphore under VUV/UV excitation," *Opt. Mat.* **31**, 131-135 (2008).
- [5] Axt, V. M. and Mukamel, S., "Nonlinear optics of semiconductor and molecular nanostructures; a common perspective", *Reviews of Modern Physics*, **70**, 145-174 (1998).
- [6] Capasso, F. and Cho , A. Y., "Bandgap engineering of semiconductor heterostructures by molecular beam epitaxy: physics and applications," *Surface Sci.* **299**, 878-891 (1994).
- [7] Taira, K., Hashimoto, T. and Yokoyama, H., "Two-photon fluorescence imaging with a pulse source based on a 980-nm gain-switched laser diode," *Optics Express* **15**, 2454-2458 (2007).
- [8] So, P. T. , Dong, C. Y., Masters, B. R. and Berland, K. M., "Two-photon excitation fluorescence microscopy," *Annu. Rev. Biomed. Eng.* **2**, 399-429 (2000).
- [9] Zipfel, W. R. , Williams, R. M. and Webb, W. W., "Nonlinear magic: multiphoton microscopy in the biosciences," *Nat. Biotechnol.* **21**, 1369-1377 (2003).
- [10] Cumpston, B.H., Ananthavel, S., Barlow, S., Dyer, D. L., Ehrlich, J.E., Erskine, L. L., Heikal, A. A., Kuebler, S. M., Lee, I. Y., McCord-Maughon, D., Qin, J., Rockel, H., Rumi, M., Wu, X. L., Marder, S. R. and Perry, J. W., "Two-photon polymerization initiators for three-dimensional optical data storage and microfabrication," *Nature*, **398**, 51 (1999).
- [11] Gattass, R.R. and Mazur, E., "Femtosecond laser micromachining in transparent materials," *Nature Photonics*, **2**, 219-223 (2008).
- [12] Ye, J. Y., Myaing, M. T., Norris, T. B., Thomas, T. and Baker Jr., J. , "Biosensing based on two-photon fluorescence measurements through optical fibers," *Opt. Lett.* **27**, 1412-1415 (2002).
- [13] Kim, H. M., Jung, C., Kim, B. R., Jung, S., Hong, J. H., Ko, Y., Lee, K. J. and Cho, B. R., "Environment-Sensitive Two-Photon Probe for Intracellular Free Magnesium Ions in Live Tissue," *Angew. Chem. Int. Ed.*, **46**, 3460–3463 (2007).
- [14] Gao, Y., Tonizzo, A., Walser, A., Potasek M. and Dorsinville, R., "Enhanced Optical Nonlinearity of Surfactant-capped CdD Quantum Dots Embedded in an Optically Transparent Polystyrene Thin Film," *Appl. Phys. Lett.* **92**, 033106-033109 (2008).
- [15] Potasek, M., "Engineered Nanostructures Exhibiting Enhanced Optical Nonlinearity," *Proc. SPIE, Quantum Dots, Particles, and Nanoclusters VI*, edited by Kurt G. Eyink, Frank Szmulowicz, Diana L. Huffaker, **7224**, 72240L1-15 (2009).
- [16] Schrödinger, E. , "An Undulatory Theory of the Mechanics of Atoms and Molecules," *Phys. Rev.* **28**, 1049–1070 (1926).
- [17] Fano, U. , "Description of States in Quantum Mechanics by Density Matrix and Operator Techniques," *Rev. Mod. Phys.* **29**, 74-93 (1957).
- [18] Sutherland, R. L., [Handbook of Nonlinear Optics], Dekker (2003).
- [19] Smith, G. D., [Numerical Solution of Partial Differential Equations: Finite Difference Methods], Oxford University Press (1985).
- [20] Parilov, E. and Potasek, M. J., "Generalized Theoretical Treatment and Numerical Method of Time-resolved Radially Dependent Laser Pulses Interacting with Multiphoton Absorbers," *J. Opt. Soc. Am B* **23**, 1894-1910 (2006).

- [21] Kim, S , McLaughlin, D., Potasek, M. J., "Propagation of the electromagnetic field in optical-limiting reverse-saturable absorbers," *Phys. Rev. A*, **61**, 025801-1-025801-4 (2000).
- [22] Potasek, M. J., Kim, S., McLaughlin, D., "All Optical Power Limiting," *J. Nonlin Opt. Phys. and Mat.*, special issue: Optical Limiters, Switches, and Discriminators: Materials, Principles and Devices, **9**, 343-364 (2000).
- [23] Parilov, E. and Potasek, M. J., "Method for Determining an Interaction Between an Electromagnetic Radiation and a Material," US Patent, 7949480 (2011).
- [24] Rogers, J. E., Slagle, J.E., McLean, D. G., Sutherland, R. L., Sankaran, B. , Kannan, R. , Tan, L.S. and Fleitz, P. A. , "Understanding the One-Photon Photophysical Properties of a Two-Photon Absorbing Chromophore," *J. Phys. Chem. A* **108**, 5514-5520 (2004).
- [25] Sutherland, R. L., Brant, M. C., Heinrichs, J. , Rogers, J. E., Slagle, J. E. , McLean, D. G. and Fleitz, P. A., " Excited-state characterization and effective three-photon absorption model of two-photon-induced excited-state absorption in organic push-pull charge-transfer chromophores ," *J. Opt. Soc. Am B* **22**, 1939 (2005).
- [26] Masunov, A., University of Central Florida, private communication, (2011)